Published in final edited form as:
J Phys Chem B. 2017 August 24; 121(33): 7899–7906. doi:10.1021/acs.jpcb.7b05568.

Nanoscale Ion Pump Derived From a Biological Water Channel

Karl Decker[†], **Martin Page**[‡], and **Aleksei Aksimentiev**[†,¶,*]
Department of Physics, Engineer Research and Development Center, Construction Engineering Research Laboratory, US Army Corps of Engineers, and Beckman Institute for Advanced Science and Technology, University of Illinois at Urbana–Champaign, Urbana, IL

Abstract

Biological molecular machines perform the work of supporting life at the smallest of scales, including the work of shuttling ions across cell boundaries and against chemical gradients. Systems of artificial channels at the nanoscale can likewise control ionic concentration by way of ionic current rectification, species selectivity, and voltage gating mechanisms. Here, we theoretically show that a voltage-gated, ion species-selective and rectifying ion channel can be built using the components of a biological water channel aquaporin. Through all-atom molecular dynamics simulations, we show that the ionic conductance of a truncated aquaporin channel non-linearly increases with the bias magnitude, depends on the channel's orientation and is highly cation specific but only for one polarity of the transmembrane bias. Further, we show that such an unusually complex response of the channel to transmembrane bias arises from mechanical motion of a positively charged gate that blocks cation transport *via* a Coulomb blockade mechanism. By combining two truncated aquaporins, we demonstrate a molecular system that pumps ions against their chemical gradients when subject to an alternating transmembrane bias. Our work sets the stage for future biomimicry efforts directed toward reproducing the function of biological ion pumps using synthetic components.

Graphical Abstract

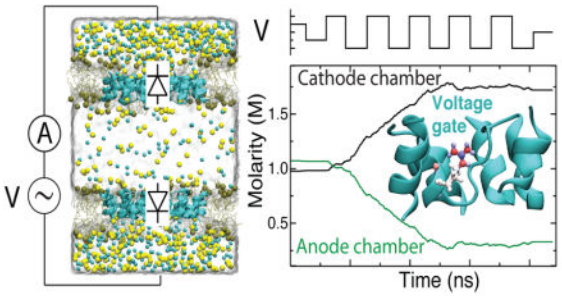

*To whom correspondence should be addressed: aksiment@illinois.edu, Telephone:+1-217-721-4764.
†Department of Physics
‡Engineer Research and Development Center
¶Beckman Institute for Advanced Science and Technology

Supporting Information Available
Plots characterizing ion currents at ±1 V bias, motion of the gate, the total charge of the anode and cathode chambers, leakage currents of fully closed and open gate, animations of the gating mechanism and pump operation. This material is available free of charge *via* the Internet at http://pubs.acs.org//

Introduction

Molecular machines in the cell operate with astonishing precision at the smallest of scales. At every moment, kinesin and myosin motors are transporting cargoes along intracellular filaments;[1] complex arrangements of proteins combine to splice target segments out of unfinished RNA;[2] and transmembrane proteins shuttle various solutes against and along their chemical gradients.[3] Fueled by voltage difference, concentration gradient, or the energy of ATP hydrolysis, these biological machines perform nanoscale work in ways and at scales beyond the reach of man-made machines. However, biological nanomachines can be and have been employed in man-made environments, as rotors[4] and in propellors,[5] driving the motion of synthetic particles. Rotors,[6] hinges,[7] membrane channels,[8] and higher-order machines[9] have also been manufactured with subnanometer precision from DNA itself. The use of biological parts in molecular engineering promises a rich future of innovation and development.

Biological and bio-inspired systems that control the transport of ions feature prominently in this promised future. Ion pumps in the body such as Na^+/K^+-ATPases alter ionic environment by shuttling individual ions of only particular species across cell membranes, and do so using ATP hydrolysis,[10–12] downhill transport of other species,[13] and conditions of alternating voltage.[1,3] Biological channels such as recently developed mutants of the α-hemolysin[14] and ompF[15] channels, conical pores in polymer membranes,[16] and solid-state diodes[17–19] can conduct ionic current with varying magnitudes based on the magnitude and direction of applied bias. The ability of these channels to regulate ionic current suggests the possibility of designing molecular machines that selectively pump ions to control ion concentration at the nanoscale.

There has been much interest in building synthetic molecular machines that mimic the function of biological molecular motors.[20–24] Efforts have included molecular walkers[22–24] and machines that imitate the ribosome to synthesize peptides from amino acids,[23,24] among others.[20,21] One way to invent such a molecular machine is to take a biological machine that already works and simplify its design until the remainder can be imitated with artificial parts.

Recently, our group used this strategy to design a small, synthetic water channel based on bovine membrane protein aquaporin-1 (AQP). The biological AQP channel is a tetramer whose four monomeric channels, Figure 1a, each permit water transport at very high rates but reject ions regardless of their species or the applied bias.[25–31] In our previous work,[32] we truncated the AQP structure to various lengths and simulated the resulting structures using the all-atom molecular dynamics (MD) method to determine the simplest design that permitted water while still rejecting ions. We found that AQP retains its function after deletion of as much as 50% of its length. Further truncation resulted in an AQP variant with only 30% the length of the original that no longer completely rejects ion transport. The more heavily truncated AQP was unsuitable as the model for an artificial water filtration channel but demonstrated potential for a different usage.

Here we show that a truncated AQP channel can be used to make a molecular ion pump. First we show that a truncated AQP exhibits hallmark properties of an ion channel: rectification of ionic current, selective ion transport and voltage gating. By combing two such channels into a double-membrane system, we demonstrate a molecular pump that could rapidly evacuate ions of both cation and anion species from one compartment to the other. Interestingly, we find the diverse response of truncated AQP to applied electric field to derive from the motion of just one amino acid side chain, suggesting a possibility of engineering a minimal synthetic molecular pump that contains only one mobile component.

Methods

Simulation Design and Protocols

An all-atom representation of a truncated AQP variant, including a modified 1-palmitoyl-2-oleoyl-sn-glycero-3-phosphoethanolamine (POPE) lipid membrane and 1 M NaCl solvent, was designed and prepared previously[32] by truncation of bovine aquaporin-1, Protein Data Bank entry 1j4n.[33] In that previous study, truncated AQP is referred to as AQP-T5, signifying it as the fifth of several truncation schemes. Our choice of the POPE-type membrane was motivated by the common use of this membrane type in experimental electrophysiological measurements. A second, double-membrane system was designed by making a copy of the first, including waters, membrane, ions, and protein, rotating it by 180° around a membrane-parallel axis, and aligning the two oppositely-facing truncated AQP along their pore axes. The centroids of the two systems were separated by the periodic cell size along the pore axis, and the new periodic cell size set to twice that of the original system, ensuring balanced solvent pressure across the membranes. Ion concentration and net ionic charge began at similar values in each of the two chambers. Including solvent, the single-membrane truncated AQP system measured $90 \times 90 \times 60$ Å^3 and contained 45,893 atoms. The double-membrane truncated AQP system measured $90 \times 90 \times 120$ Å^3 and contained 91,674 atoms.

All MD simulations were performed using molecular dynamics program NAMD[34] and CHARMM36[35] parameters for atomic interactions supplemented by NBFix corrections to accurately describe nonbonded ion-protein interactions.[36] Particle mesh Ewald full electrostatics[37] computed over a cubic grid with spacing < 1.2 Å^3, and a smooth (7–8 Å^3) cutoff for van der Waals interactions were implemented for evaluation of the non-bonded forces, which were evaluated at each 2 fs simulation timestep. All simulations were carried out using rigid hydrogen bonds[38,39] and periodic boundary conditions. The temperature was held constant using the Lowe-Andersen thermostat,[40] rate 50 ps^{-1}, at 310 Kelvin. The TIP3P water model[41] was used in each simulation. All minimizations used the conjugate gradient method.

After its creation from two opposite-facing single-membrane systems, the double-membrane system was minimized and then equilibrated for 1 ns. Equilibration was performed in the constant number of particles, pressure and temperature ensemble at 1 atm pressure enforced by the Langevin piston extendible along the pore axis, with decay and period of 800 fs each; the systems' dimensions within the plane of the membrane (xy plane) were confined to

remain at a 1:1 ratio. All simulations under applied electric field were carried out in the constant number of particles, volume and temperature ensemble.

Restraint forces, employed using the constraints feature of NAMD, maintained the protein and lipid bilayer shape and integrity system for all simulations. As in previous work,[32] the carbon atoms of the lipid bilayers were restrained, and α-carbon atoms in the protein were harmonically restrained to their crystallographic coordinates. These restraints were applied during production simulation as well as equilibration. The spring constant of each restraint was 2 kcal mol^{-1} $Å^{-2}$.

Visualization and analysis were performed using VMD.[42]

Ionic Current and Conductance Measurements

Ionic current and conductance were measured using systems containing 1 M NaCl buffer and time-dependent transmembrane bias. The transmembrane bias was induced by applying an external electric field perpendicular to the membrane.[43] Single-membrane truncated AQP was run at alternating voltages of ±1 V, switching polarity every 20–40 ns, for a total of 950 ns. Starting in each case from the final coordinates of this run, the system was simulated again at ±500 mV, ±800 mV, and ±1200 mV for ~300 ns at each magnitude of bias, or ~150 ns at each specific voltage. Double-membrane truncated AQP was run for 850 ns under varying bias.

To compute integrated ionic current, the sodium and chloride ions that completely crossed each membrane under constant bias were summed and the resulting sums multiplied by sodium and chloride charge, respectively. The integrated current was divided by the elapsed simulation time and the result averaged over the several periods of constant bias to produce the mean and standard deviation of current. The mean conductance was found by dividing the mean current by the applied bias. Instantaneous current was found by numerical differentiation of the integrated current: at each timestep, the integrated current was subtracted from the integrated current for the next timestep and the result divided by the size of the timestep.

Results & Discussion

The truncated AQP channel, Figure 1b, was obtained by removing the majority of the length of the wild-type AQP. Each monomer in the AQP tetramer was truncated in this way to make a truncated AQP tetramer. A lipid bilayer already equilibrated to wild-type AQP was truncated to make the height of the bilayer closer to the height of the truncated AQP, so as to reduce the risk of lipid invasion of the pores as seen in previous work.[44] 1 M NaCl solvent was added on either side of the membrane. The system was minimized to eliminate steric conflicts between atoms and equilibrated for 1 ns to produce the complete system shown in Figure 1c,d. A detailed description of the simulation procedures is given in Methods.

To characterize the ion conducting properties of truncated AQP we simulated the truncated AQP tetramer embedded in a lipid membrane under varying transmembrane bias conditions. Figure 2a illustrates a typical simulation: the transmembrane bias was switched periodically

between +500 and −500 mV over the 300 ns duration of the simulation. Since every atom was modeled explicitly, the current carried by ion transport through the four monomeric truncated AQP channels was measured by simply counting the ions as they crossed the membrane. Under ±500 mV bias, truncated AQP exhibited limited ion conductivity, with the average current produced being of the same scale as thermal transport. Increasing the magnitude of the transmembrane bias to 800 and and then to 1200 mV produced a considerable increase in the ionic current, Figure 2b,c. Note that the transmembrane bias range of ±1V is typical for experimental studies of synthetic ion channels.[17] Comparing these traces to those for ±500 mV reveals that the current rises suprlinearly with applied bias, a phenomenon known as voltage gating. In addition, these current traces demonstrate a markedly larger current at negative applied bias (as shown in Figure 1c) than positive applied bias, meaning that truncated AQP rectifies ionic current.

Assessing the mean of the observed currents only made the rectification more apparent. A time-average was taken of the current measured during each section of trajectory with constant polarity of bias. Taking the mean of these time-averages produces Figure 2d, revealing strong dependence of current magnitude on polarity of bias. Rectification as a ratio of the magnitude of negative and positive current is quantified in the inset to Figure 2e; these ratios are comparable with those of other biological and solid-state nanoscale rectifying systems characterized both experimentally[15,16,45,46] and *in silico*.[46,47] Taking the absolute value of current and dividing by applied bias to obtain the conductance proves, further, that conductance itself varies nonlinearly with bias magnitude as well as polarity, Figure 2e. Variance of conductance on bias magnitude suggests truncated AQP is not merely a rectifier, but a voltage gating diode for current. Previously, some voltage-gated biological channels[48,49] have been found to depend on a mechanism for gating called the Coulomb blockade;[50,51] at the nanoscale, this phenomenon depends on manipulation of the local ionic concentrations based on charges presented by the nanopore. Others voltage-gated channels depend on electrowetting[52] of the pore or actually open to allow current and close to prevent it.[53]

The dependence of ionic conductance on applied bias only becomes more striking when NaCl current is broken down in terms of transport by ion species, Cl^- and Na^+, as shown in Figure 3a–c and Figure S1c. These permeation traces show that Cl^- moves back and forth across truncated AQP while Na^+ moves almost strictly in one direction. Analyzing the transport again in terms of ionic current, Na^+ conductance at negative biases is larger than than of Cl^- and dwarfs Na^+ conductance at positively biases, Figure 3d–e. The rectification of ionic current through truncated AQP is selective to cations particularly. Bias-sensitive modulation of Na^+ current points to a gating mechanism responsive to bias; rectification of cations particularly suggests a positively charged gate that electrostatically blocks cation transport when the gate is closed.

To identify the species-specific, rectifying gate mechanism, we examined ionic current traces of Na^+ and Cl^- in response to alternating 1000 mV bias, Figure 4a–c. Na^+ current through truncated AQP typically flatlines within nanoseconds of changes in the polarity of applied bias, Figure 4b. Cl^- current merely changes direction. Review of the simulation trajectory reveals a positively charged group that responds to changes in polarity on a similar

timescale: the rotamer of the sidechain of Arg-197, one of the residues thought to enforce rejection of ions in wild-type AQP.[54–56] Mutation of protein nanopore residues to arginine was shown to lead to a conformation-based gating mechanism that enforces rectification in α-hemolysin;[14] the motion of a single, charged residue was shown to gate ionic current through the OccK channels.[57] Figure 4d shows the z-coordinate of the Arg-197 guanidine group. The z-coordinate of this positively charged group is seen to alternate between two stable states and to change in response to the change of the bias polarity. In the state characterized by the stable and positive z coordinate, Figure 4e, the electrostatic barrier presented by positively charged Arg-197 prevents permeation of positively charged Na^+ but not Cl^-. The gate is then closed; Na^+ ions only rarely pass. In the state characterized by the stable and negative z coordinate, Figure 4f, Arg-197 is far from its crystallographic conformation, the gate is open, and Na^+ ions pass more readily. The gate responds to the change of the transmembrane bias polarity on the nanosecond timescale; SI Movie 1 illustrates the gating process. Thus, voltage-induced conformational changes in the arginine residue produce a one-way gate for Na^+ current through the nanochannel. The motion of the gate, however, does not have a dramatic effect on the Cl^- current. Plots of the transmembrane electrostatic potential profile through the selectivity filter of the channel in the open and closed states, Figure S2, indicates that ionic conductance is mechanically gated in the high-voltage regime.

In addition to the gate and its motion, there is evidence that gating of truncated AQP also benefits from a ionic Coulomb blockade. As shown in Figure S3, the 500 mV and 800 mV biases fail to close the gates as effectively as at 1200 mV. Yet, Na^+ current varies nonlinearly with voltage even considering only the data from $\pm$500 mV and $\pm$800 mV, Figure 3. In this way truncated AQP resembles other biological channels known to gate current due to the manipulation of local ionic concentration by the charges of the pore,.[50,51] Certainly, the channel is not observed to empty of water in the way of previously made channels,[44,52] ruling out electrowetting.

The monodirectional transport of Na^+ through truncated AQP suggests the possibility of evacuating ions from one solvent reservoir to another. In all previously described simulations, however, excess Na^+ merely moved across the periodic boundary without altering NaCl molarity. Instead, we brought a molecular pump to life by using two copies of the diode-like truncated AQP tetramer and arranging the tetramers to point in opposite directions, Figure 5a. In the language of diodes, the anodes of both tetramers share a solvent reservoir called the “anode” chamber and the cathodes share the other solvent reservoir, or “cathode” chamber. Upon assembly, the system was minimized and then equilibrated for 1 ns, which was sufficient to attain equilibrium volume.

We began our investigation of the double-membrane truncated AQP system by simulating it under $\pm$1 V bias, ~60 ns for each bias polarity, Figure 5b. The simulation produced negligible ion currents. This result could be expected as the voltage bias drop across each membrane was only 500 mV, which we previously found to be insufficient to produce significant current across the truncated AQP diode in either direction, Figure 2a. To demonstrate feasibility of ion pumping, the system was then simulated for 600 ns under a 2 V-magnitude bias alternating every 60 ns. During this simulation, Na^+ current was seen to

flow from anode to cathode across the truncated AQP diode whose orientation matches the polarity of bias. Cl^- current proceeded in the opposite direction across both tetramers, Figure 5b–c, but more Cl^- left the anode chamber than entered it. In this way the anode chamber was rapidly emptied of ions, until roughly 530 ns of simulation have passed, Figure 5d. Thus, anti-aligned truncated AQP tetramers can function as ionic diodes, allowing alternating applied bias to evacuate the majority of the chamber's ions despite leakage.

Ultimately, leakage across the truncated AQP diodes does inhibit further evacuation of ions. Note that over the course of the simulation, the net positive charge of the anode chamber gradually increases, Figure S4; Na^+ leakage into the anode chamber doesn't increase because of ion-induced transmembrane bias, but rather in spite of it. In the single-membrane system, NaCl current across truncated AQP is rectified, with the ratio of currents at ± 1 V bias being 4.1 ± 0.2 in favor of current at negative bias. Na^+ current at ± 1 V bias is more heavily rectified, with a ratio of currents of 13.6 ± 11.7, again in favor of current at negative bias. As the molarity ratio of NaCl in the two chambers increases, current from the more concentrated cathode-facing chamber can be expected to increase proportionately while current from the anode-facing chamber can be expected to decrease. This means that ions will have to move more and more through the closed gate. Indeed, when the Na^+ current through the closed gate and Na^+ current through the open gate are considered as a ratio, that ratio increases from 0.0044 ± 0.003 to 0.58 ± 0.3 when comparing the first 400 ns to the last 400 ns of simulation time. The result is the tapering-off of the molarity ratio of NaCl in the two chambers seen in Figure 5e. By the end of nearly 900 ns simulation, the ratios of molarity in the two chambers don't quite reach the maximum denoted by the ratio of Na^+ currents seen in the single-membrane system at 1 V bias, but they well exceed the ratio of total current at that bias. The highly stochastic nature of leakage events makes estimation of the dynamic equilibrium state of the molarity from relatively short MD simulation somewhat challenging. In addition, note that the currents through both single-membrane and double-membrane truncated AQP measured in this study include periods where the Arg-197 gate is in the process of responding to switched polarity of bias. The current measurements then include leakage across an effectively misfunctioning voltage gate. The maximum rectification of current across single-membrane truncated AQP and the maximum molarity ratio of the double-membrane truncated AQP could both be higher with less frequent bias switching, see Figure S5.

Conclusions

In summary, we have shown that truncated AQP can function as a voltage-gated, anion-specific ionic current rectifier, where Coulomb blockade and mechanical gating, but not electrowetting,[52,58] serve to regulate the ionic current. By placing two oppositely oriented truncated AQP in separate membranes, we built a molecular pump that could evacuate ions from one solvent chamber to the other in response to an alternating electric field. Future improvements to truncated AQP's function as a voltage-gated ionic pump could involve chemical modifications of the Arg-197 gate, point mutations of other residues critical to wild-type AQP function,[54,55] and tuning the electrostatic environment by changing the type of a lipid bilayer membrane. MD simulations of the gating charge[59] could greatly facilitate such efforts. By adding a second, anion-selective gate, the truncated AQP system could be

transformed into a charge separation system that, subject to an alternating transmembrane bias, would generate an electro-chemical gradient that could be used to power other membrane-embedded systems. Another exciting possibility is development of a membrane gate that facilitates or inhibits transport of a particular cation or anion species, which could find application in purification and remediation technologies. Due to the difficulty of truncating an existing protein structure without causing unfolding, practical applications of such biologically-inspired membrane systems would necessitate the use of biomimicry to reproduce the chemical architecture and physical properties of truncated AQPs using robust and modular synthetic components.[60]

Supplementary Material

Refer to Web version on PubMed Central for supplementary material.

Acknowledgments

This work was supported by the US Army under the Engineer Research and Development Center's Environmental Quality and Installations business area and by the National Institutes of Health (P41-RR005969). The authors acknowledge supercomputer time provided through the ERDC High Performance Computing Center at Vicksburg, Mississippi, XSEDE Allocation Grant MCA05S028 and the Blue Waters petascale supercomputer system at the University of Illinois at Urbana-Champaign.

References

1. van den Heuvel MGL, Dekker C. Motor Proteins at Work for Nanotechnology. Science. 2007; 317:333–336. [PubMed: 17641191]
2. Will CL, Lührmann R. Spliceosome Structure and Function. Cold Spring Harb Perspect Biol. 2011:3.
3. Schrempf H, OS, Kümmerlen R, Hinnah S, Müller D, Betzler M, Steinkamp T, Wagner R. A Prokaryotic Potassium Ion Channel with Two Predicted Transmembrane Segments from Streptomyces Lividans. EMBO J. 1995; 14:5170–5178. [PubMed: 7489706]
4. Bachand GD, Montemagno CD. Constructing Organic/Inorganic NEMS Devices Powered by Biomolecular Motors. Biomedical Microdevices. 2000; 2:179–184.
5. Soong RK, Bachand GD, Neves HP, Olkhovets AG, Craighead HG, Montemagno CD. Powering an Inorganic Nanodevice with a Biomolecular Motor. Science. 2000; 290:1555–1558. [PubMed: 11090349]
6. Ketterer P, Willner EM, Dietz H. Nanoscale Rotary Apparatus Formed from Tight-Fitting 3D DNA Components. Sci Adv. 2016; 2:e1501209. [PubMed: 26989778]
7. Funke JJ, Dietz H. Placing Molecules with Bohr Radius Resolution Using DNA Origami. Nat Nanotech. 2016; 11:47–52.
8. Langecker M, Arnaut V, Martin TG, List J, Renner S, Mayer M, Dietz H, Simmel FC. Synthetic Lipid Membrane Channels Formed by Designed DNA Nanostructures. Science. 2012; 338:932–6. [PubMed: 23161995]
9. Marras AE, Zhou L, Su HJ, Castro CE. Programmable Motion of DNA Origami Mechanisms. Proc Natl Acad Sci U S A. 2015; 112:713–718. [PubMed: 25561550]
10. Astumian RD. Stochastic Conformational Pumping: A Mechanism for Free-Energy Transduction by Molecules. Annu Rev Biophys. 2011; 40:289–313. [PubMed: 21351880]
11. Serpersu EH, Tsong TY. Activation of Electrogenic Rb+ Transport of (Na,K)-ATPase by an Electric Field. J Biol Chem. 1984; 259:7155–7162. [PubMed: 6327708]
12. Xie TD, der Chen Y, Marszalek P, Tsong TY. Fluctuation-Driven Directional Flow in Biochemical Cycle: Further Study of Electric Activation of Na,K Pumps. Bio-phys J. 1997; 72:2496–2502.

13. Gadsby DC. Ion Channels Versus Ion Pumps: the Principal Difference, in Principle. Nature. 2009; 10:344–352.
14. Maglia G, Heron AJ, Hwang WL, Holden MA, Mikhailova E, Li Q, Cheley S, Bayley H. Droplet Networks with Incorporated Protein Diodes Show Collective Properties. Nat Nanotech. 2009; 4:437–440.
15. Miedema H, Vrouenraets M, Wierenga J, Meijberg W, Robillard G, Eisenberg B. A Biological Porin Engineered Into a Molecular, Nanofluidic Diode. Nano Lett. 2007; 7:2886–2891. [PubMed: 17691852]
16. Siwy ZS, Fuliński A. Origin of $1/f^{a}$ Noise in Membrane Channel Currents. Phys Rev Lett. 2002; 89:158101. [PubMed: 12366027]
17. Vlassiouk I, Siwy ZS. Nanofluidic Diode. Nano Lett. 2007; 7:552–556. [PubMed: 17311462]
18. Daiguji H, Oka Y, Shirono K. Nanofluidic Diode and Bipolar Transistor. Nano Lett. 2005; 5:2274–2280. [PubMed: 16277467]
19. Shankla M, Aksimentiev A. Modulation of Molecular Flux Using a Graphene Nanopore Capacitor. J Phys Chem B. 2017; 121:3724–3733. [PubMed: 28009170]
20. Cheng C, McGonigal PR, Stoddart JF, Astumian RD. Design and Synthesis of Nonequilibrium Systems. ACS Nano. 2015; 9:8672–8688. [PubMed: 26222543]
21. Coskun A, Banaszak M, Astumian RD, Stoddard JF, Grzybowski BA. Great Expectations: Can Artificial Molecular Machines Deliver on Their Promise? Chem Soc Rev. 2012; 41:19–30. [PubMed: 22116531]
22. von Delius M, Geertsema EM, Leigh DA. A Synthetic Small Molecule that Can Walk Down a Track. Nat Chem. 2010; 2:96–101. [PubMed: 21124398]
23. Lewandowski B, De Bo G, Ward JW, Papmeyer M, Kuschel S, Aldegunde MJ, Gramlich PME, Heckmann D, Goldup SM, D'Souza DM, et al. Sequence-Specific Peptide Synthesis by an Artificial Small-Molecule Machine. Science. 2013; 339:189–193. [PubMed: 23307739]
24. He Y, Liu DR. Autonomous Multistep Organic Synthesis in a Single Isothermal Solution Mediated by a DNA Walker. Nat Nanotech. 2010; 5:778–782.
25. Zhu F, Tajkhorshid E, Schulten K. Theory and Simulation of Water Permeation in Aquaporin-1. Biophys J. 2004; 86:50–57. [PubMed: 14695248]
26. Fei Z. A Synthetic Zwitterionic Water Channel: Characterization in the Solid State by X-Ray Crystallography and NMR spectroscopy. Angew Chem Int Ed Engl. 2005; 44:5720–5725. [PubMed: 16059949]
27. Yu J, Yool AJ, Schulten K, Tajkhorshid E. Mechanism of Gating and Ion Conductivity of a Possible Tetrameric Pore in Aquaporin-1. Structure. 2006; 14:1411–1423. [PubMed: 16962972]
28. Kaucher MS. Selective Transport of Water Mediated by Porous Dendritic Dipeptides. J Am Chem Soc. 2007; 129:11698–11699. [PubMed: 17784763]
29. Duc YL. Imidazole-Quartet Water and Proton Dipolar Channels. Angew Chem Int Ed Engl. 2011; 50:11366–11372. [PubMed: 22002728]
30. Hu XB, Chen Z, Tang G, Hou JL, Li ZT. Single-Molecular Artificial Transmembrane Water Channels. J Am Chem Soc. 2012; 134:8384–8387. [PubMed: 22574988]
31. Zhou X. Self-Assembling Subnanometer Pores with Unusual Mass-Transport Properties. Nat Commun. 2012; 3:949. [PubMed: 22805556]
32. Decker K, Paige M, Boyd A, MacAllister I, Ginsberg M, Aksimentiev A. Selective Permeability of Truncated Aquaporin 1 In Silico. ACS Biomater Sci Eng. 2017; 3:342–348.
33. Sui H, Han BG, Lee JK, Walian P, Jap BK. Structural Basis of Water-Specific Transport Through the AQP1 Water Channel. Nature. 2001; 414:872–878. [PubMed: 11780053]
34. Phillips JC, Braun R, Wang W, Gumbart J, Tajkhorshid E, Villa E, Chipot C, Skeel RD, Kale L, Schulten K. Scalable Molecular Dynamics with NAMD. J Comput Chem. 2005; 26:1781–1802. [PubMed: 16222654]
35. Brooks BR, MacKerell AD Jr, Nilsson L, Petrella RJ, Roux B, Won Y, Archontis G, Bartels C, Boresch S, Caflisch A, et al. CHARMM: the Biomolecular Simulation Program. J Comput Chem. 2009; 30:1545–614. [PubMed: 19444816]

36. Yoo J, Aksimentiev A. Improved Parametrization of Li^+, Na^+, K^+, and Mg^{2+} Ions for All-Atom Molecular Dynamics Simulations of Nucleic Acid Systems. J Phys Chem Lett. 2012; 3:45–50.
37. Darden TA, York D, Pedersen L. Particle Mesh Ewald: An N log(N) Method for Ewald Sums in Large Systems. J Chem Phys. 1993; 98:10089–92.
38. Miyamoto S, Kollman PA. SETTLE: An Analytical Version of the SHAKE and RATTLE Algorithm for Rigid Water Molecules. J Comput Chem. 1992; 13:952–962.
39. Andersen HC. Rattle - a Velocity Version of the Shake Algorithm for Molecular-Dynamics Calculations. J Comput Phys. 1983; 52:24–34.
40. Koopman EA, Lowe CP. Advantages of a Lowe-Andersen Thermostat in Molecular Dynamics Simulations. J Chem Phys. 2006; 124:204103. [PubMed: 16774315]
41. Jorgensen WL, Chandrasekhar J, Madura JD, Impey RW, Klein ML. Comparison of Simple Potential Functions for Simulating Liquid Water. J Chem Phys. 1983; 79:926–935.
42. Humphrey W, Dalke A, Schulten K. VMD: Visual Molecular Dynamics. J Mol Graphics. 1996; 14:33–38.
43. Aksimentiev A, Schulten K. Imaging α-Hemolysin with Molecular Dynamics: Ionic Conductance, Osmotic Permeability and the Electrostatic Potential Map. Biophys J. 2005; 88:3745–3761. [PubMed: 15764651]
44. Shen YX, Si W, Erbakan M, Decker K, Zorzi RD, Saboe PO, Kang YJ, Majd S, Butler PJ, Walz T, et al. Highly Permeable Artificial Water Channels That Self-Assemble into Two-Dimensional Arrays. Proc Natl Acad Sci U S A. 2015; 112:9810–9815. [PubMed: 26216964]
45. Menestrina G. Ionic Channels Formed by Staphylococcus aureus Alpha-Toxin: Voltage-Dependent Inhibition by Divalent and Trivalent Cations. J Membrane Biol. 1986; 90:177–190. [PubMed: 2425095]
46. Gamble T, Decker K, Plett TS, Pevarnik M, Pietschmann JF, Vlassiouk I, Aksimentiev A, Siwy ZS. Rectification of Ion Current in Nanopores Depends on the Type of Monovalent Cations: Experiments and Modeling. J Phys Chem C. 2014; 118:9809–9819.
47. Cruz-Chu ER, Aksimentiev A, Schulten K. Ionic Current Rectification Through Silica Nanopores. J Phys Chem C. 2009; 113:1850–1862.
48. Corry B, Thomas M. Mechanism of Ion Permation and Selectivity in a voltage gated sodium channel. J Am Chem Soc. 2012; 134:1840–1846. [PubMed: 22191670]
49. Payandeh J, Scheuer T, Zheng N, Catterall W. The Crystal Structure of a Voltage-Gated Sodium Channel. Nature. 2011; 475:353–358. [PubMed: 21743477]
50. Krems M, Ventra MD. Ionic Coulomb Blockade in Nanopores. J Phys: Condens Matter. 2013:25.
51. Kaufman IK, McClintock PVE, Eisenburg RS. Coulomb Blockade Model of Permeation and Selectivity in Biological Ion Channels. New J Phys. 2015:17.
52. Trick JL, Song C, Wallace EJ, Sansom MSP. Voltage Gating of a Biomimetic Nanopore: Electrowetting of a Hydrophobic Barrier. ACS Nano. 2017; 11:1840–1847. [PubMed: 28141923]
53. Tagliazucchi M, Szleifer I. Transport Mechanisms in Nanopores and Nanochannels: Can We Mimic Nature? Materials Today. 2015; 18:131–142.
54. Tajkhorshid E, Nollert P, Jensen MØ, Miercke LJW, O'Connell J, Stroud RM, Schulten K. Control of the Selectivity of the Aquaporin Water Channel Family by Global Orientational Tuning. Science. 2002; 296:525–530. [PubMed: 11964478]
55. Chen H, Wu Y, Voth GA. Origins of Proton Transport Behavior from Selectivity Domain Mutations of the Aquaporin-1 Channel. Biophys J. 2006; 90:L73–L75. [PubMed: 16581846]
56. Wang Y, Tajkhorshid E. Molecular Mechanisms of Conduction and Selectivity in Aquaporin Water Channels. The Journal of Nutrition. 2007; 137:1509S–1515S. [PubMed: 17513417]
57. Pothula KR, Dhanasekar NN, Lamichhane U, Younas F, Pletzer D, Benz R, Winterhalter M, Kleinekathöfer U. Single Residue Acts as Gate in OccK Channels. J Phys Chem B. 2017; 121:2614–2621. [PubMed: 28257208]
58. Powell MR, Cleary L, Davenport M, Shea KJ, Siwy ZS. Electric-Field-Induced Wetting and Dewetting in Single Hydrophobic Nanopores. Nat Nanotech. 2011; 6:798–802.
59. Roux B. The Membrane Potential and its Representation by a Constant Electric Field in Computer Simulations. Biophys J. 2008; 95:4205–4216. [PubMed: 18641071]

60. Vaddypally S, Xu C, Zhao S, Fan Y, Schafmeister CE, Zdilla MJ. Architectural Spiroligomers Designed for Binuclear Metal Complex Templating. Inorg Chem. 2013; 52:6457–6463. [PubMed: 23668771]

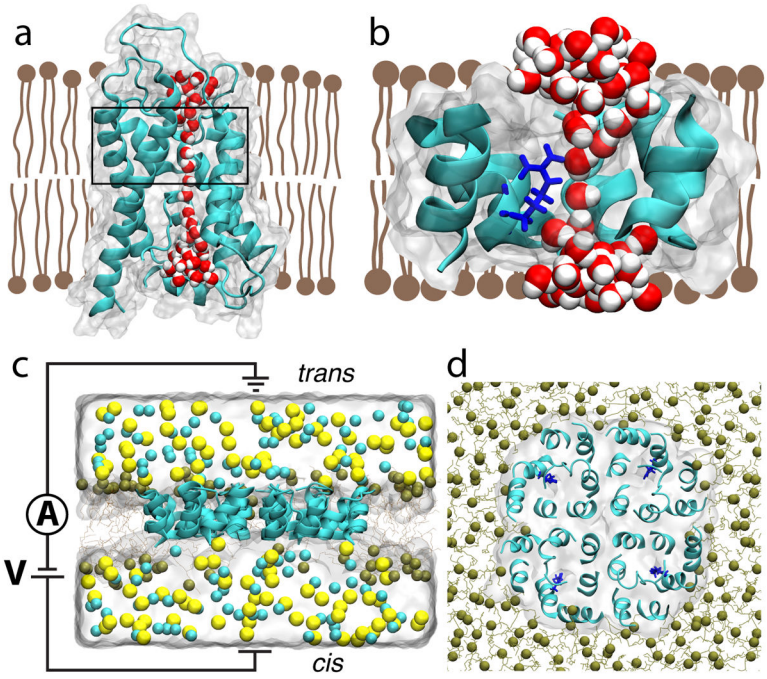

Figure 1.

All-atom model of truncated aquaporin. (a,b) Side-on view of wild-type aquaporin monomer (panel a) and its truncated version (panel b). The secondary structure of the AQP proteins is shown using a cartoon representation; each protein's boundaries are depicted by a semi-transparent molecular surface. The lipid bilayer is shown as brown schematic, and the water wire through the AQP monomers is shown using red (oxygen) and white (hydrogen) spheres. In panel a, the region to be left after truncation of the protein is indicated by a black rectangle. In panel b, residue Arg-197 is additionally shown in blue licorice. To provide a better view of the water wire, certain residues of the proteins are not shown. (c,d) Side (panel c) and top (panel d) views of the system used to characterize ion conductance of truncated AQP. Ochre lines and spheres illustrate the truncated POPE membrane (spheres represent the phosphorous atoms of lipids); the semi-transparent surface illustrates the volume occupied by 1 M NaCl electrolyte; Na^+ and Cl^- ions are depicted as yellow and cyan spheres, respectively. For clarity, electrolyte is not shown in the top view of the system. The circuit diagram in panel c indicates applied bias and measurement of transmembrane ionic current.

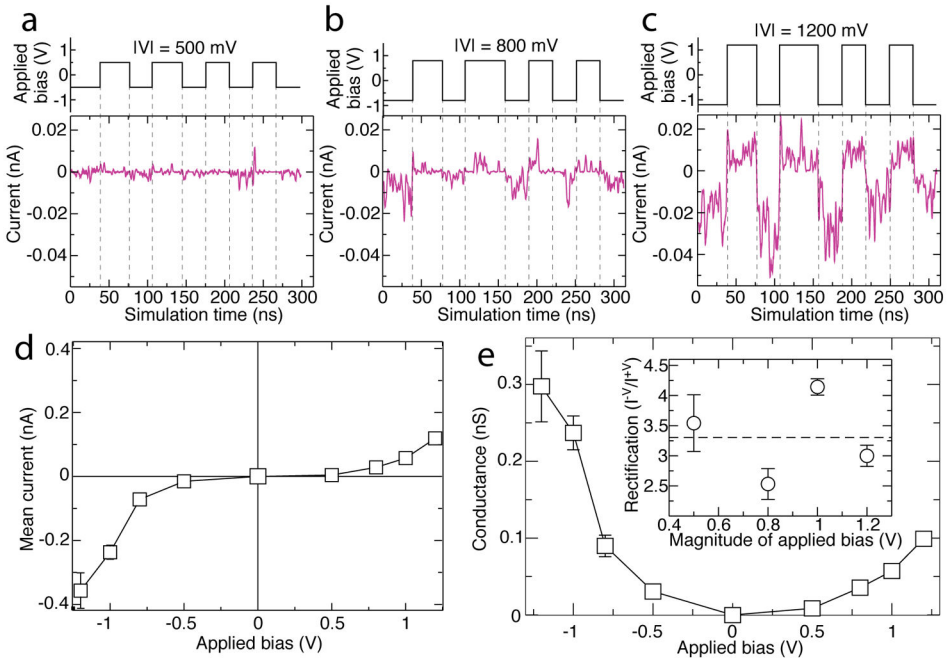

Figure 2.

Ionic current, conductance, and rectification of truncated AQP system. (a–c) Ionic current across truncated AQP embedded in a lipid membrane, Figure 1c,d, at ±500 mV, ±800 mV, and ±1200 mV biases respectively, with magnitude of bias given as —V— at the top of each panel. Data at ±1000 mV are reported in Figure S1. Purple traces indicate current whereas step-function black traces indicate the applied transmembrane bias *versus* simulation time. The ionic current traces show 2 ns running average of the instantaneous current sampled every 9.6 ps. Dashed lines serve as guides for the eye. Positive current travels from *cis* to *trans* as defined in Figure 1c. (d,e) Mean ionic current (d) and ion conductance (e) of the truncated AQP tetramer as a function of transmembrane bias. Mean current is calculated by, first, finding the time-average of the ionic current across the tetramer for each constant bias fragment of the trajectory. The weighted average of these currents is the mean current reported. Error bars in both panels indicate the standard deviation of the mean. The mean conductance and its standard deviation are found by dividing mean current by magnitude of applied bias. The inset of (e) shows the ratios of the current at negative biases to the current at the corresponding positive biases. Error bars specify the propagated standard deviations in the mean currents.

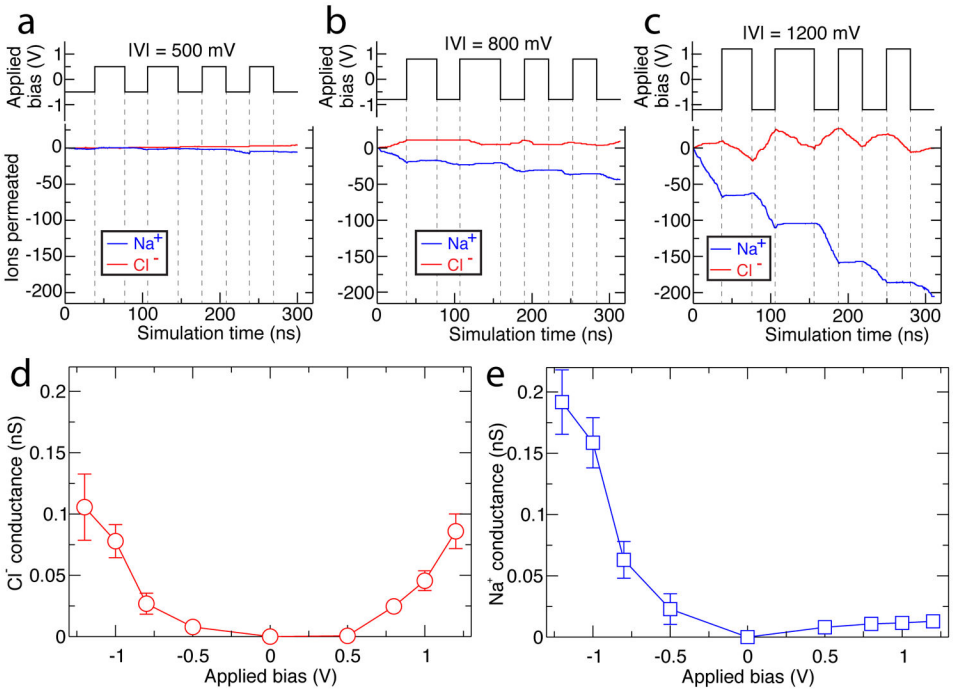

Figure 3.

Species-specific ionic conductance of truncated AQP. (a–c) The number of ions permeated across the truncated AQP tetramer system at ±500 mV, ±800 mV, and ±1200 mV biases respectively, with magnitude of bias given as —V— at the top of each panel. Red traces indicate Cl^- permeation, blue traces indicate Na^+ permeation. Step-function black traces indicate the applied transmembrane bias *versus* simulation time, with dashed lines serving as guides for the eye. Data at ±1000 mV are reported in Figure S1. (d–e) Mean Cl^- (d) and Na^+ (e) conductance of the truncated AQP tetramer. Error bars indicate the standard deviation of the mean conductance. The mean values were computed as described in the caption to Figure 2.

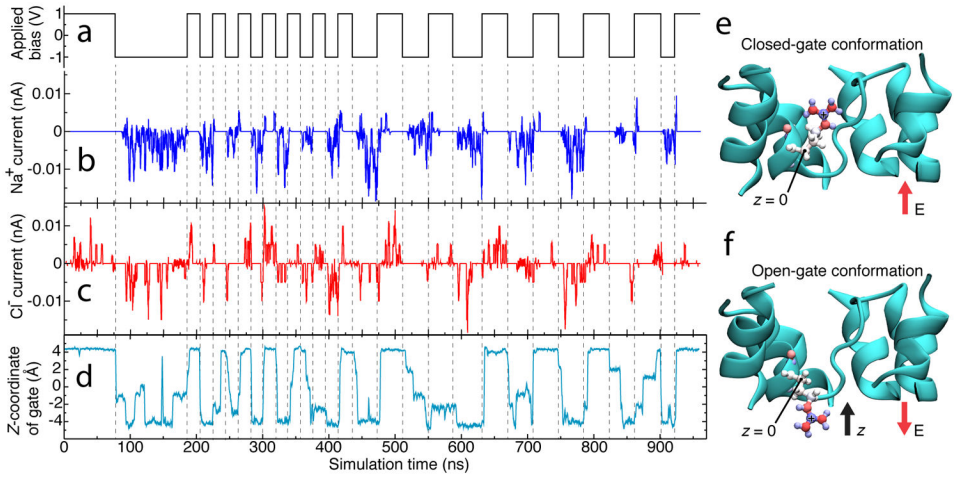

Figure 4.

Mechanism of species-specific gating in truncated AQP. (a–d) Correlation of applied bias (a) and Na^+ (b) and Cl^- (c) currents through one of the monomers of the truncated AQP tetramer, compared with displacement of that monomer's Arg-197 side chain (d). In panel d, the location of the Arg-197 side chain is characterized by the *z*-coordinate of the chain's guanadine group. Dashed lines serve as guides to the eye. The *z* axis is defined in panels e and f. (e,f) Molecular mechanism of truncated AQP gating. The terminal carbon in the positively charged guanadine group of Arg-197 is pictured in blue with a "+" on it. Arg-197, the residue responsible for gating, is rendered as spheres and sticks colored according to individual atomic charge (blue for positive, red for negative). At positive bias (panel e), the channel is closed, at negative bias (panel f) it is open. The direction of electric field is shown with red arrows, the direction of the *z*-axis is shown with a black arrow, and the location of the carbon atom whose position constitutes $z = 0$ is labeled. The truncated AQP is shown in cyan; water, ions, lipids, and one protein alpha-helix are omitted for clarity.

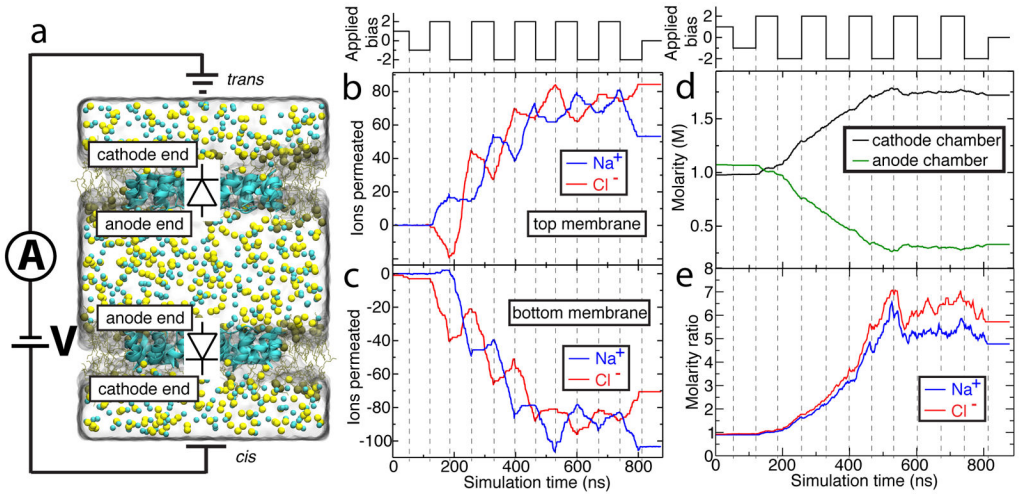

Figure 5.

Performance of an ion pump built using truncated AQP. (a) Simulation system with parts depicted as in Figure 1c. In this double-membrane system, the bottom truncated AQP tetramer is oriented as in Figure 1c, while the top complex faces opposite. Because of the opposing orientations, the gate residues of one tetramer remain closed while those of the other are open. Note that the use of periodic boundary conditions means that the upper and lower partitions depicted here function as single chamber, referred to as the cathode chamber. (b–c) The number of ions permeated through the top (b) and bottom (c) truncated AQP tetramers of the double-membrane system as a function of the simulation time. The step-function black trace above panel b indicates the applied bias. Ion permeation across either membrane in the *cis* to *trans* direction (defined in panel a) increases the ion count; transport in the opposite direction decreases it. Na^+ overwhelmingly travels from the anode (center) chamber to the cathode (outer two partitions) chamber in response to applied bias for as long as the gates remain effective. Dotted lines serve as guides for the eye. (d) Molarity of NaCl in the anode (green) and cathode (black) chambers. The step-function black trace above panel d indicates the applied bias. (e) Ratio of Na^+ (blue trace) and Cl^- (red trace) molarity in the cathode chamber to that of the anode chamber.